AUT Journal of Electrical Engineering

AUT J. Elec. Eng., 58(1) (2026) 189-204
DOI: 10.22060/eej.2025.24499.5717

Design of Three-Phase Grid-Connected PV System with Z-Source Boost Converter and Neural Network-Based Harmonic Elimination

B. Kavya Santhoshi[1,*], Dondapati Ravi Kishore[2], Md. Shoaib Akhter[1], Asif Iqubal1, Ashraf Ali[1]

[1] Department of Electrical & Electronics Engineering, Godavari Institute of Engineering and Technology (A), Rajahmundry, India.
[2] Department of Electrical & Electronics Engineering, Godavari Global University, Rajahmundry, India.

ABSTRACT: The progress towards Renewable Energy Sources (RESs) has highlighted the crucial role of Photovoltaic (PV) systems in meeting the energy demands of the world. As energy from PV systems becomes significant, there is need for efficient and high-quality grid systems becomes essential. As a consequence, this research proposes a grid-connected PV system to address the challenges by integrating a Z-Source Boost Converter (ZSBC) and a neural network-based controller for eliminating harmonics. The ZSBC is employed to overcome the limitations of conventional DC-DC converters, offering greater flexibility in voltage boosting and improved reliability in power conversion. Additionally, the system utilizes a Cascaded Adaptive Neuro-Fuzzy Inference System (ANFIS) based Maximum Power Point Tracking (MPPT) controller to ensure that the PV array operates at its maximum efficiency under all conditions, thereby maximizing energy harvest. To continue high power quality and ensure grid compliance, the system incorporates a DQ-based Artificial Neural Network (ANN) controller. The system validation is carried out using MATLAB, with results demonstrating superior performance in terms of 96.42% converter efficiency and 1.23% Total Hormonic Distortion (THD). This innovative approach not only improves the overall efficiency and reliability but also ensures that it meets the requirements of modern grids.

Review History:

Received: Jul. 31, 2025
Revised: Nov. 07, 2025
Accepted: Dec. 02, 2025
Available Online: Jan. 10, 2026

Keywords:

Photovoltaic
ZSBC
Cascaded ANFIS MPPT
DQ-based ANN Controller
Harmonic Elimination

1- Introduction

The gradual progress of small-scale RESs into the power grid has been driven by their economic, technical, and environmental advantages, even though larger power plants offer several benefits [1, 2]. Solar PV systems are a particularly attractive option since they convert sunlight directly into electrical energy using power electronics. These systems are either connected to grid-tied or stand-alone units [3]. Nevertheless, before the implementation of a solar PV system [4], it is crucial to address constraints imposed by existing power generation infrastructure, for ensuring stable and reliable performance under normal operations and during grid faults.

Enhancing PV voltage for compatible grid operation necessitates the utilization of DC-DC converters. Traditionally used Boost converter [5] steps up the input voltage, but is limited by the maximum duty cycle and reduced efficiency at higher voltages. The Buck-Boost converter [6] increases or decreases voltage, but inverts the polarity, adding design complexity and resulting in higher switching losses. The Cuk converter [7] both step up/ down the voltage while maintaining polarity, but its complex design with extra inductors and capacitors increases size, leading to higher component stress and lower efficiency at high power levels. The Single Ended Primary Inductor Converter (SEPIC) [8] allows non-inverted voltage stepping up or down but has a complex design with a higher component count and causes EMI issues. To overcome these challenges, modified converters have been introduced. The improved quadratic boost converter, combined with switch-capacitor cell structure [9], offers ultra-high voltage gain without an additional doubler circuit. This reduces the component count, with lower voltage stress and offers continuous source current. But, still requires careful design and control to manage the high voltage gain and ensure stability. The cascaded modified Cuk converter [10] uses a cascade design with three cells to accomplish improved gain in voltage. Nevertheless, an increased number of components results in higher losses in voltage and necessitates careful design for maintaining higher efficiency. Another, often used converter is Z-source inverter [11, 12] developed for addressing limitations of voltage and current source inverters with its unique impedance network. This allows for both boosting of voltage and single-stage inversion. But demands sophisticated control strategies to handle shoot-through states and to accomplish boosting of voltage. In addition, the passive components in the topology introduce issues of Electromagnetic Interference (EMI). In response to these challenges, this work introduces a novel ZSBC as a superior

*Corresponding author's email: kavyabe2010@gmail.com

alternative.

Renewable energy systems, specifically PV, utilize MPPT for optimal extraction of power. Among the most frequently used traditional approaches are Perturb and Observe (P&O) [13], which increases the system power continuously in the same direction. While P&O technique is simple, leads to suboptimal performance. The Incremental Conductance (InCond) [14, 15], is performed by examining the slope of the power curve in relation to voltage, but results in slower convergence at the MPP, and is also difficult for Partial Shading Condition (PSC). Addressing these limitations, the intelligent MPPT techniques have gained importance, using algorithms including Artificial Neural Network (ANN) [16, 17], Fuzzy Logic [18], ANFIS [19], which utilize linguistic variables and rules to track the MPP. The major benefits of these techniques include handling system non-linearity and uncertainty without any precise control. Anyhow, designing an effective logic controller necessitates expert knowledge and proper tuning to optimal performance. Overwhelming the limitations of this approach, this paper utilized Cascaded ANFIS MPPT, owing to their faster convergence and better adaptability to dynamic environmental scenarios.

Efficient generation of compensating current for VSI is crucial to improve the quality of power. This paper designs a DQ theory-based ANN to eliminate the harmonics and control the PCC voltage. The key contributions of the proposed work include:

Implementing a novel ZSBC for handling low voltage outputs from the PV system and enhancing system efficiency under variable load conditions.

Incorporation of Cascaded ANFIS-MPPT algorithm significantly improves the tracking speed and accuracy, specifically under changing PV scenarios.

The combination of dq theory and ANN controller enhances harmonic detection and suppression, providing a faster and more adaptive response to grid variations and nonlinear loads.

The system's d-q assisted ANN control allows for managing both active and reactive power, enhancing grid stability and improving the system's ability to regulate voltage and frequency.

The paper proceeds with section II presenting the proposed methodology, section III detailing the modelling of system components, section IV covering results and discussion part and section, section V presenting comparison of proposed and existing methods, VI summarizes the conclusion.

2- Proposed System Description

The proposed system demonstrates a three-phase (3Φ) grid-tied PV system designed to efficiently transform solar energy into electrical power for integration into utility grid, shown Figure 1. The DC electricity from PV is fed to ZSBC, which helps boost the voltage level for the grid integration connection. To ensure the PV system operates at its Maximum Power Point (MPP), Cascaded ANFIS-based MPPT is integrated. Controller dynamically adjusts the operating condition of PV array, offering reference signals to control the subsequent power conversion stages.

The attained DC voltage is converted to AC via 3Φ Voltage Source Inverter (VSI) to be synchronized with the grid in terms of voltage, frequency, and phase. To ensure the AC output is of high quality, it passes via an LCL filter,

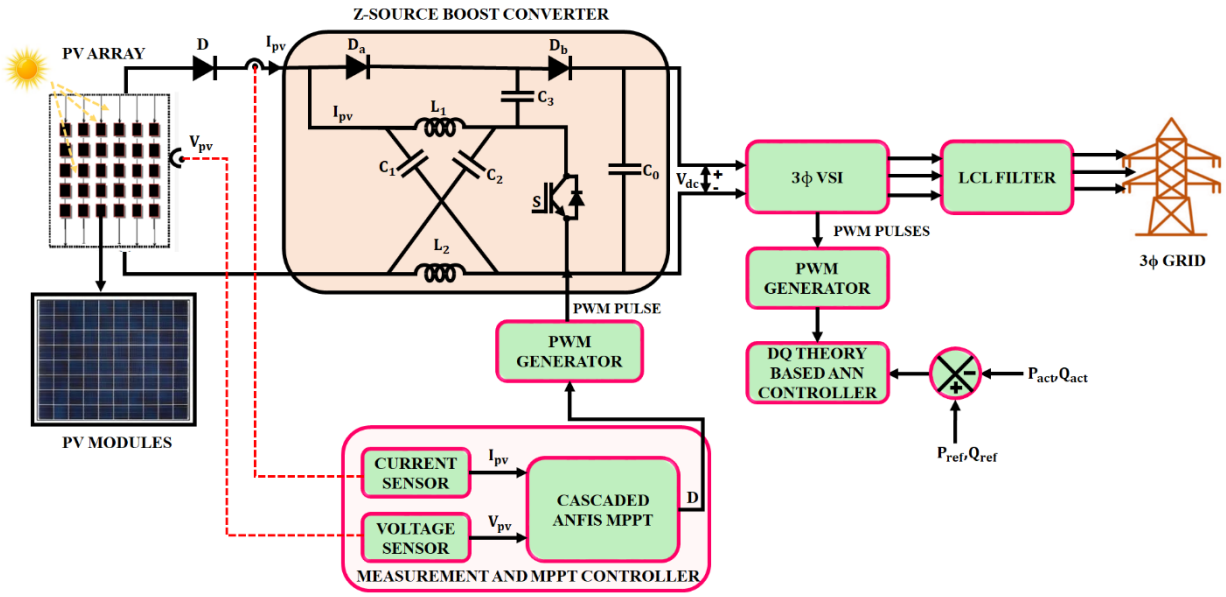

Fig. 1. Proposed System PV Grid System.

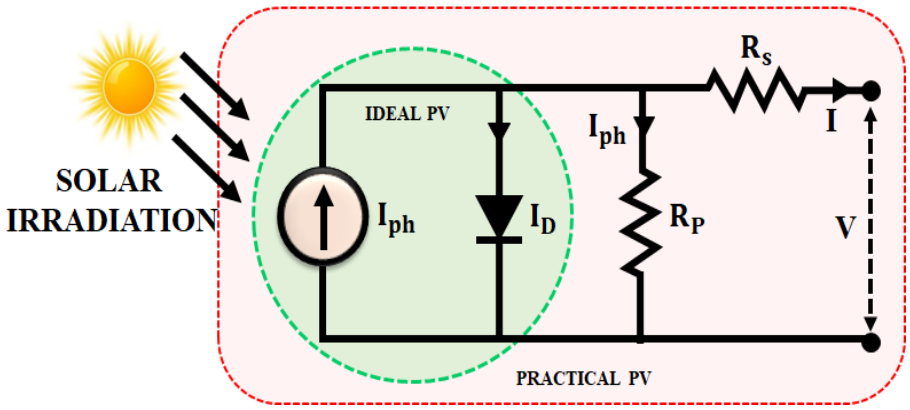

Fig. 2. Circuit of a Single Diode PV Module

eliminating high-frequency switching harmonics. The filtered AC output is fed to a grid managed by a dq theory-based ANN controller. The controller monitors the actual and reactive power output and adjusts the inverter's PWM signals to minimize harmonics. This results in ensuring the power delivered to the grid meets the desired specifications.

3- Methodology

3- 1- Mathematical Modelling of PV System

The research utilizes PV as a source for generating energy. The main purpose of a PV system is to stimulate electrical output based on solar irradiance and temperature. A PV cell model is illustrated in Figure 2.

The single diode model is widely adopted. On applying Kirchhoff's current law, the output current is mathematically expressed as Eq (1):

$$I_{out} = I_{ph} - I_0 \left\{ \left[\frac{q\left(V_{out} + I_{out} R_s\right)}{AKT_c} \right] - 1 \right\} - \frac{V_{out} + I_{out} R_s}{R_p} \quad (1)$$

Where output current is represented as I_{out} and voltage as V_{out}. The diode saturation current and photocurrent is indicated I_0 and I_{ph}. Resistance linked in series and parallel as R_s and R_p. Moreover, the electron charge is stated as q, ideality factor by A, Boltzmann's constant as K, and absolute temperature as T_c. However, the voltage for PV source is low, and necessitates DC-DC converter for optimal boosting.

3- 2- Operation of Z-Source Boost Converter

In the proposed work, a novel ZSBC is presented, shown in Figure 3, which overcomes the limitations of traditional boost and Z-source converters. The developed converters offer higher voltage gain with decreased component stress.

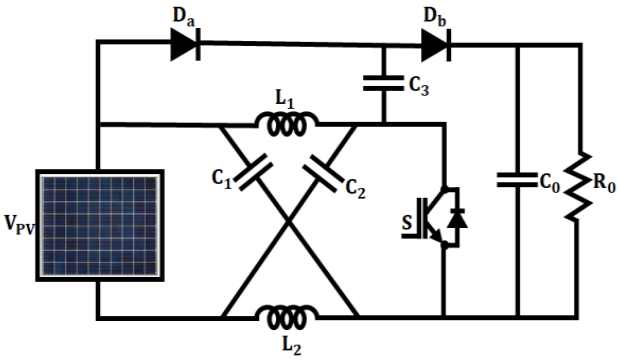

Fig. 3. Proposed circuit of ZSBC

The developed converter integrates shoot-through states, resulting in short circuit avoidance and enhanced reliability.

In the operating mode illustrated in Figure 4(a), both the diode D_b and switch S are in the ON state, while the diode D_a is deactivated, allowing energy to be stored in inductors L_1 and L_2. The diode D_a blocks the reverse current from the input, allowing to flow in one direction. And, the diode D_b blocks the current flowing to the load.

$$V_{PV} - V_{L_1} + V_{C_2} = 0 \quad (2)$$

$$V_{PV} + V_{C_2} - V_{L_2} = 0 \quad (3)$$

$$V_{C_3} = 0 \quad (4)$$

During this mode diode D_b and Switch S are in OFF state, displays in Figure 4(b) the stored energy in inductors L_1 and L_2, is released to load through inductors C_3,C_0 and

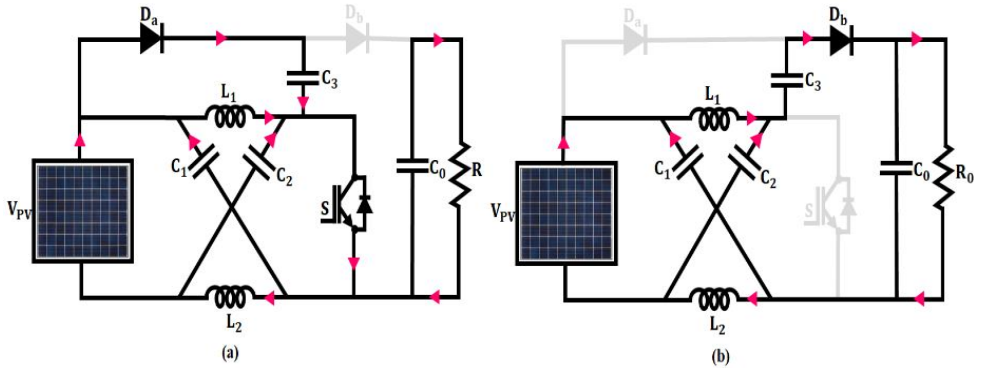

Fig. 4. Operation of ZSBC (a) Switch ON State and (b) Switch OFF State.

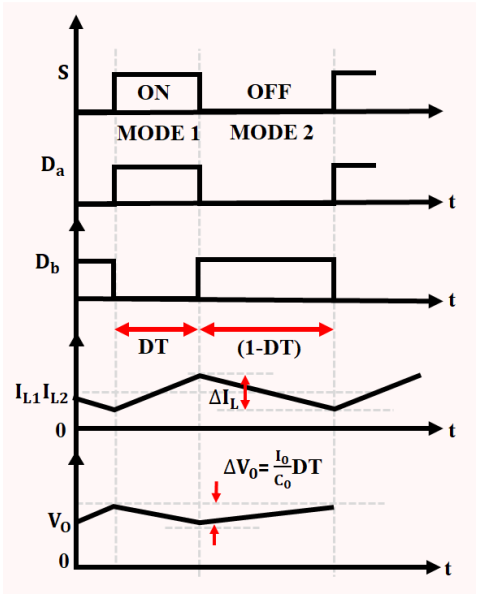

Fig. 5. Switching Waveform of Proposed Converter.

D_b. The Z-source network boosts the voltage, transferring energy from inductors and capacitors to output. The diode D_a is reverse-biased, blocking the input current from flowing back to the source. On applying KVL,

$$V_{L_1} = -V_{C_1} \tag{5}$$

$$V_{L_2} = -V_{C_2} \tag{6}$$

$$V_{PV} + V_{C_1} + V_{C_2} + V_{C_3} = 0 \tag{7}$$

To clearly derive voltage gain, the operation of converter is analyzed in both ON and OFF states. During the ON state, the inductor voltages are,

$$V_{L_1} = V_{in} \tag{8}$$

$$V_{L_2} = V_{in} \tag{9}$$

During the OFF state, the stored inductor energy is released, giving:

$$V_{L_1} = V_{in} - V_{C_1} \tag{10}$$

$$V_{L_2} = V_{in} - V_{C_2} \tag{11}$$

The principle of volt-second balance to inductor L_1, using Equations (2) and (5), while assuming that $C_1 = C_2$ the expression becomes

$$\left(V_{C_2} + V_{PV}\right)D - V_{C_1}\left(1-D\right) = 0 \tag{12}$$

$$V_{C_1} = \frac{D\left(V_{C_2} + V_{PV}\right)}{1-D} \tag{13}$$

$$V_{C_1} = V_{C_2} = \frac{DV_{PV}}{1-2D} \tag{14}$$

$$V_o = V_{C_1} + V_{C_2} = \frac{2V_{in}}{1-D} \tag{15}$$

On substitution of Equation (14) in (7), the voltage gain Expression becomes,

$$\frac{V_0}{V_{PV}} = \frac{2-2D}{1-2D} \tag{16}$$

Here, V_{in} is the input voltage from V_{PV}, V_o stands output voltage analog converter (V), D represents duty ratio, L_1 and L_2 are inductors, C_1 and C_2 are the capacitors, i_{L1} and i_{L2} represents inductor currents, V_{C_1} and V_{C_2} denotes capacitor voltages, T_s is the switching period (s). Figure 5 illustrates a timing waveform of the proposed converter. The ZSBC effectively improves system stability and voltage gain, making it suitable for PV applications. To enhance the system performance further, integration of MPPT algorithm is essential.

3- 3- Cascaded ANFIS MPPT Technique

The Cascaded ANFIS MPPT, which comprises of two ANFIS structures shown in Figure 6, is modelled to optimize the power output from the PV system. The system ensures the process of PV at its MPP under changing conditions. ANFIS is effective in modelling complex non-linear functions by adjusting its parameters using input-output data. Its five layers are,

Fuzzification Layer: In this layer, the input membership grades are generated, and for a given input x and its corresponding fuzzy set A_i, the output is estimated as,

$$O_i^1 = \mu_{A_i}(x) \tag{17}$$

Where, $\mu_{A_i}(x)$ is the membership function.

Rule Layer: Every neuron in this layer resembles to a fuzzy rule combining the input's membership values. For two inputs x and y,

$$O_i^2 = \omega_i = \mu_{A_i}(x) \cdot \mu_{B_i}(y) \tag{18}$$

Where, ω_i is the firing strength of rule i.

Normalization Layer: In this layer, the firing strength of the rules are normalized.

$$O_i^3 = \bar{\omega}_i = \frac{\omega_i}{\sum_{j=1}^{N} \omega_j} \tag{19}$$

Here, $\bar{\omega}_i$ denotes normalized firing strength. N stands total number of fuzzy rules.

Defuzzification Layer: In this layer, a linear function is applied to the inputs, which is weighted by the normalized firing strength.

$$O_i^4 = \bar{\omega}_i \cdot (p_i x + q_i y + r_i) \tag{20}$$

Where, p_i, q_i and r_i are the parameters that have to be learned. x *and* y are the input variables to the ANFIS.

Output Layer: In this layer, the final output is produced by combining the outputs of all rules.

$$O^5 = \sum_{i=1}^{N} \bar{\omega}_i \cdot (p_i x + q_i y + r_i) \tag{21}$$

In Cascaded ANFIS, two ANFIS networks act in unison to optimize the duty cycle of PV fed converter to ensure MPP operation.

First ANFIS Stage

The first ANFIS takes PV voltage (V_{PV}) and current (I_{PV}) as inputs to control the initial change in the duty cycle (ΔD_1). The input-output relationship for the first ANFIS is modelled as,

$$\Delta D_1 = f_1(V_{PV}, I_{PV}) \tag{22}$$

Here, ΔD_1 stands change in the duty cycle estimated

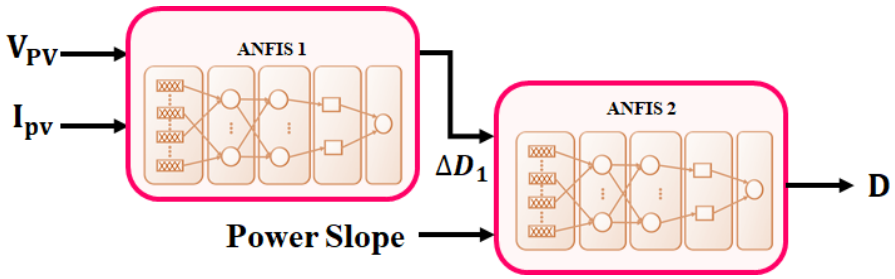

Fig. 6. Structure of Cascaded ANFIS

from the first ANFIS stage based on PV voltage (V_{PV}) and PV current (I_{PV}). The output ΔD_1 is estimated as the defuzzified output from the ANFIS model,

$$\Delta D_1 = \sum_{i=1}^{N} \omega_i^{-1} \left(p_i^1 V_{PV} + q_i^1 I_{PV} + r_i^1 \right) \tag{23}$$

Second ANFIS Stage

In the second ANFIS stage, the output of the first stage is refined by considering ΔD_1 and the power slope $\left(\frac{dP_{PV}}{dV_{PV}}\right)$

$$\Delta D = \sum_{i=1}^{N} \omega_i^{-2} \left(p_i^2 \Delta D_1 + q_i^2 \frac{dP_{PV}}{dV_{PV}} + r_i^2 \right) \tag{24}$$

Where,

$$\frac{dP_{PV}}{dV_{PV}} = I_{PV} + V_{PV} \cdot \frac{dI_{PV}}{dV_{PV}} \tag{25}$$

The power slope offers an understanding of the relationship between power and voltage, which in turn helps the system to optimize the duty cycle. To ensure replicability, the ANFIS structure is defined as follows. Each stage consists of five layers: fuzzification, rule, normalization, defuzzification, and output. In this case, triangular membership functions are used with three membership functions defined for each input variable (V_{PV} ,I_{PV} ,, and power slope $\frac{dP_{PV}}{dV_{PV}}$). The fuzzy rule base, consisting of 9 IF-THEN rules, in each stage allows effective mapping between inputs and a shift in the duty cycle. The training dataset is created from simulated PV characteristics under varying irradiance $(800-1000W/m^2)$ and temperature $(20-40°C)$, producing nearly 10,000 iterations. The dataset is divided into training (70%), validation (15%), and testing (15%). The combination of least-squares assessment and gradient descent is used to fit parameters for fast convergence and tune rules effectively. This structure helps the system converge faster to the MPP by effectively using the feedback from the first ANFIS output.

3- 4- DQ theory-based ANN Controller

The proposed work utilizes a theory-based ANN controller for ensuring efficient control of both active and reactive power in a developed PV-grid system. These advanced control techniques offer accurate regulation of power and mitigation of harmonics. The control process starts by sensing the 3φ voltage (V_a, V_b, V_c) and current (i_a, i_b, i_c) signals from the system. These signals are then handled using a Phase Locked Loop (PLL) to produce sine and cosine signals, to ensure that the reference frame aligns with the grid voltage for optimal control.

By applying Park's transformation the 3φ current gets converted into dq frame. This transformation rotates the reference frame in synchronization with the grid voltage. The transformation from the coordinates of $\alpha\beta$ into dq frame is given by

$$\begin{bmatrix} i_d \\ i_q \end{bmatrix} = \begin{bmatrix} cos\theta & sin\theta \\ -sin\theta & cos\theta \end{bmatrix} \begin{bmatrix} i_\alpha \\ i_\beta \end{bmatrix} \tag{26}$$

Where current components of dq frame is noted as i_d and i_q, with i_d corresponding to active power and reactive power as i_q. The system's goal is to regulate actual power output to match desired reference values for both active and reactive power. The actual power values are calculated as:

$$\Delta P = P_{ref} - P_{act} \tag{27}$$

$$\Delta Q = Q_{ref} - Q_{act} \tag{28}$$

The error signals ΔP and ΔQ are inputs to the ANN controller, which uses its learning and adaptive capabilities to compute the required control actions. This is crucial for non-linear system dynamics, where conventional control methods might struggle. The ANN adapts based on historical data and real-time conditions, ensuring optimal control of the PWM signals for the VSI. Once ANN processes the control signal, the reverse Park transformation is applied for the conversion of dq signals back to abc reference frame for the generation of appropriate reference signals for the PWM generator. The reverse transformation is expressed by

$$\begin{bmatrix} i_\alpha \\ i_\beta \end{bmatrix} = \begin{bmatrix} cos\theta & -sin\theta \\ sin\theta & cos\theta \end{bmatrix} \begin{bmatrix} i_{ddc} \\ i_{qdc} \end{bmatrix} \tag{29}$$

Here, $i_\alpha, and\ i_\beta$ are transformed into current components in the stationary $\alpha-\beta$ frame. For the generation of reference current in abc frame, the following transformation is used

$$\begin{bmatrix} i_{sa}^* \\ i_{sb}^* \\ i_{sc}^* \end{bmatrix} = \begin{bmatrix} 1 & 0 \\ 1/2 & \sqrt{3}/2 \\ 1/2 & -\sqrt{3}/2 \end{bmatrix} \begin{bmatrix} i_\alpha \\ i_\beta \end{bmatrix} \tag{30}$$

The reference current signals are indicated as i_{sa}^*, i_{sb}^* and $i_s c^*$, are used to control the switching pulses of VSI. The ANN controller is based on a multi-layer feedforward neural network structure. It has an input layer with two neurons corresponding to the error signal $(\Delta P\ and\ \Delta Q)$, followed by two hidden layers, which contain 15 and 10 neurons. The tansigmoid activation function operates in hidden layers,

Table 1. System Specification.

Component	Symbol	Specification
PV System		
Maximum Power	P_{max}	10kW
No.of Cells in Series	N_S	3
No.of Cells in Parallel	N_P	15
Voltage at P_{MPP}	V_{MPP}	29.95V
Current at P_{MPP}	I_{MPP}	8.35Amps
Short Circuit Current	I_{SC}	8.95Amps
Open Circuit Voltage	V_{OC}	37.25V
Irradiance	G	$1000 W / m^2$
Temperature	T	35℃
ZSBC		
Capcitor	C_1, C_2, C_3	$22\mu F$
Output Capcitor	C_0	$2200\mu F$
Inductor	L_1, L_2	$4.7mH$
Switching Frequency	f_s	$10kHz$
Input voltage	V_{in}	80V
Output voltage	V_{out}	900V
Grid and filter		
Grid voltage	V_{grid}	415V
Grid frequency	f_{grid}	$50Hz$
Filter type	-	*LCL filter*
Filter inductance	Lf	$2mH$
Filter capacitance	Cf	$50\mu F$
Simulation Measurement		
Simulation solver	-	Ode45
Step time	-	0.2s

while a linear activation function operates in the output layer to generate control signals. The Levenberg-Marquardt backpropagation algorithm is used for training, which has fast convergence properties when applied to nonlinear control problems. The training dataset for the ANN controller is developed from simulation data of the PV-grid system at different loads and irradiance conditions. This simulation dataset had a total of 12,000 samples, and was split into a training (70 %), validation (15 %), and testing (15 %) set. Combination of dq theory and ANN ensure precise regulation of active and reactive power, improving power quality through reducing harmonic distortion and enhancing grid stability. The ANN controller's learning capability allows it to adapt to system changes (e.g., fluctuating solar irradiance in PV systems) more efficiently than traditional controllers.

4- Results and Discussion

This section explores a microgrid system integrating a ZSBC, along with a Cascaded ANFIS MPPT controller, which is discussed. Additionally, the system's capability to step up voltage from PV, tracking of MPPT, and mitigation of harmonics is also evaluated under varying conditions. Table 1 offers the key specifications of system components. A comprehensive assessment of the converter's effectiveness in the elimination of harmonics is also discussed.

The system is assessed under two different environmental states, as outlined in Table 2. Case 1 represents steady-state working conditions, such as irradiance $1000 W / m^2$ and $25°C$, while case 2 represents dynamically changing conditions with step changes in irradiance and temperature, simulating realistic partial shading and atmospheric variations. These test scenarios provide comprehensive validation of the

Table 2. Experimental/Simulation Environmental Conditions.

Case	Time (s)	Irradiance (W/m^2)	Temperature (℃)	Operating condition
Case 1	0-0.5	1000	35	Constant irradiance and temperature
Case 2	0-0.2	800	25	Reduced irradiance, constant temperature
Case 2	0.2-0.3	800	35	Temperature step increase
Case 2	0.3-0.5	1000	35	Irradiance step increase

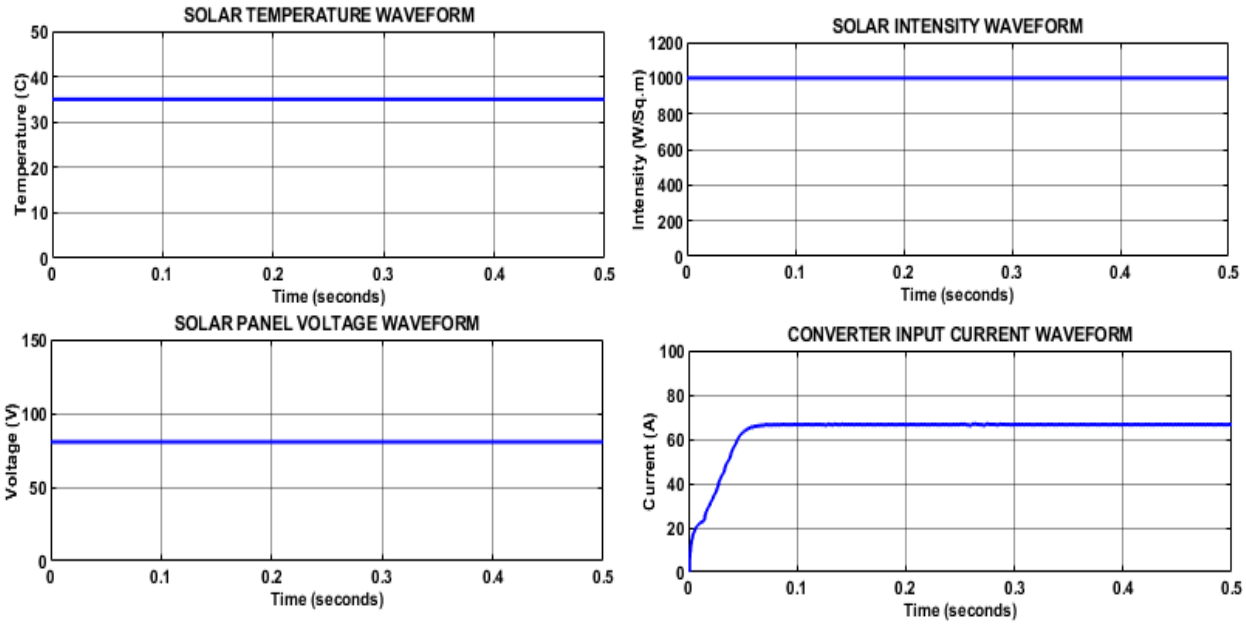

Fig. 7. PV Performance at Steady State Condition.

system's performance characteristics under stable and quickly changing operating environments.

Case 1: Steady State Condition

To analyse the performance of the developed system, at first, the performance is examined under constant conditions of temperature and intensity, shown in Figure 7. It is noted that the temperature is maintained at a constant of $35℃$, with irradiance at $1000W/m^2$. In response to this steady state condition, the PV panel continues with a constant voltage of 80V, with current showing initial rise and maintained at 65A, without any further oscillations. Under this condition, response of proposed converter is demonstrated in Figure 8.

The proposed converter shows an enhanced voltage level from the input voltage. It is noticed that a step-up voltage of 900V is attained after 0.1s with an initial rise. Similarly, followed by initial variations, a stabilized current of 5.4A is accomplished. This determines the superiority of the developed converter in boosting the voltage.

Case 2: Fluctuating condition

Similarly, to know the effectiveness of the developed system, it is also examined under varying conditions shown in Figure 9. The temperature waveform shows constant performance with $25℃$ till 0.2s, after the temperature rises and continues at $25℃$, without any further changes. Meanwhile, the intensity is sustained at $800W/m^2$, till 0.3s, after the intensity level rises and follows as $1000W/m^2$. According to this scenario, the voltage observed by PV panel shows a step response in voltage level and finally continues

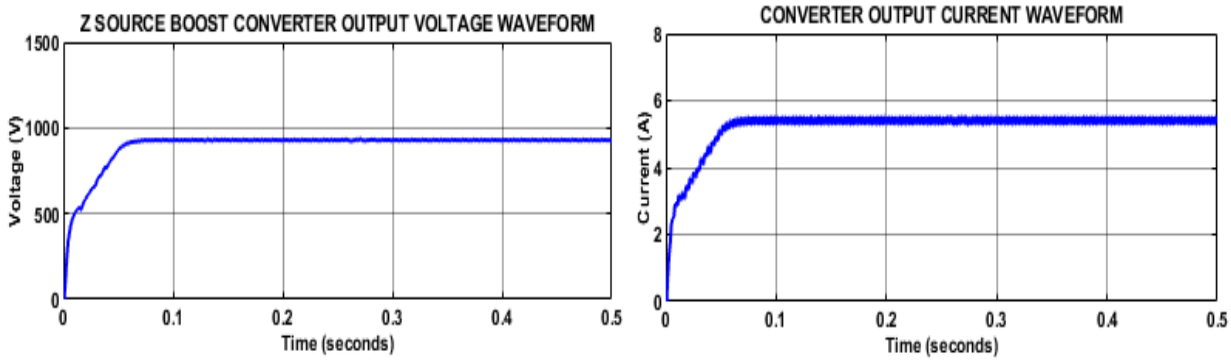

Fig. 8. Proposed ZSBC Output Waveform.

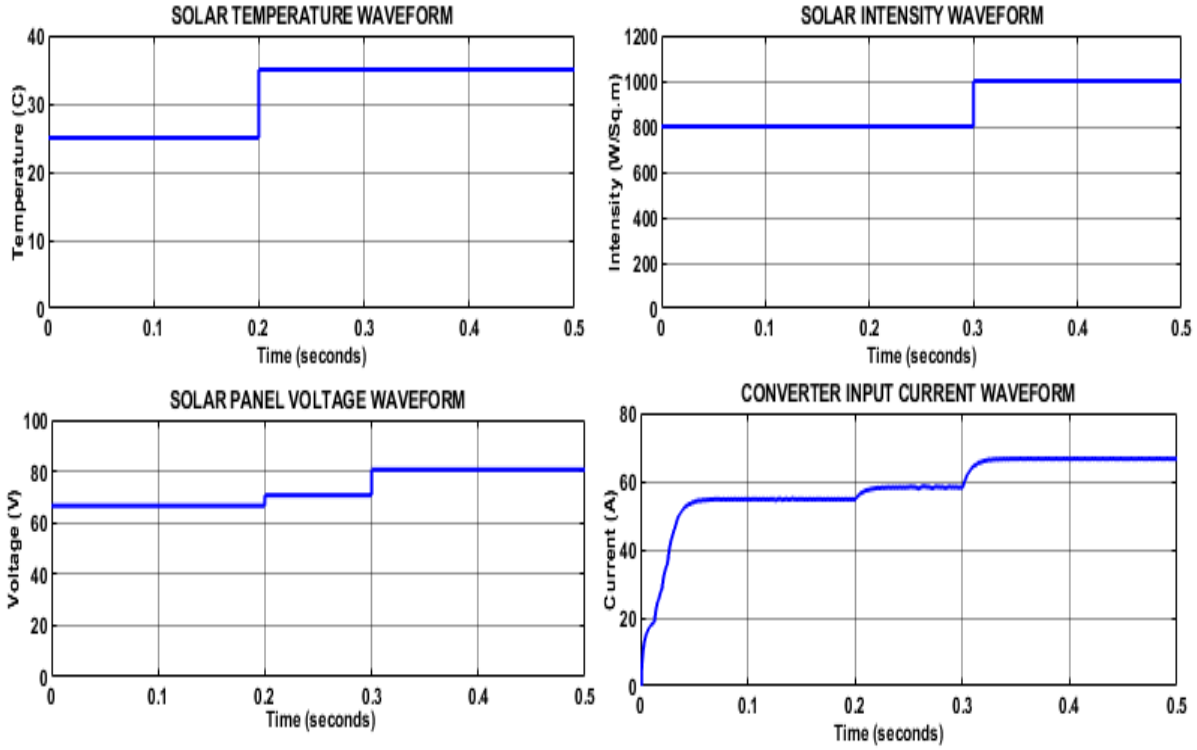

Fig. 9. PV Performance at Varying Environmental Conditions.

at 80V. In correspondence, the input current to the converter shows same step variations and continues at 63A, after 0.32s.

For the condition of changing temperature and intensity, the proposed converter shows step distinctions in voltage and current, shown in Figure 10. However, the converter effectively boosts the level of voltage and continues at 900V after 0.33s, without any further. Whereas, the current waveform of the proposed converter maintains a constant value of 5.4A after 0.33s, which initial step change.

For the developed system, the power response under changing temperature and conditions is shown in Figure 11. It is noticed that an input power measure of 5040W is observed, followed by the converter output power of 4860W, which is the MPP accomplished with the assistance of the Cascaded ANFIS MPPT approach.

For the developed 3Φ grid system, the accomplished voltage, current, and in-phase response are explained in Figure 12. It is observed that a steady voltage of 415V is applied with a current of 12A. This shows that the performance of the ANN controller is achieving stabilized grid performance. Moreover, the in-phase waveform demonstrates the synchronization of voltage and current delivered to the grid.

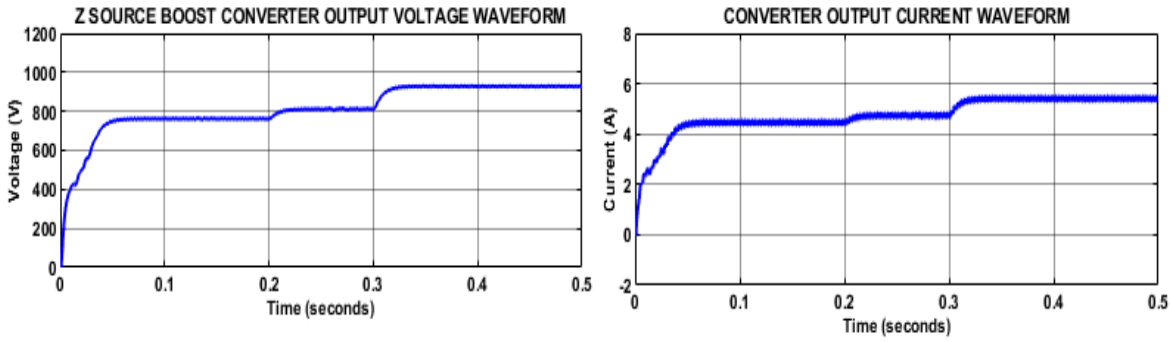

Fig. 10. Converter Performance at Varying Environmental Conditions.

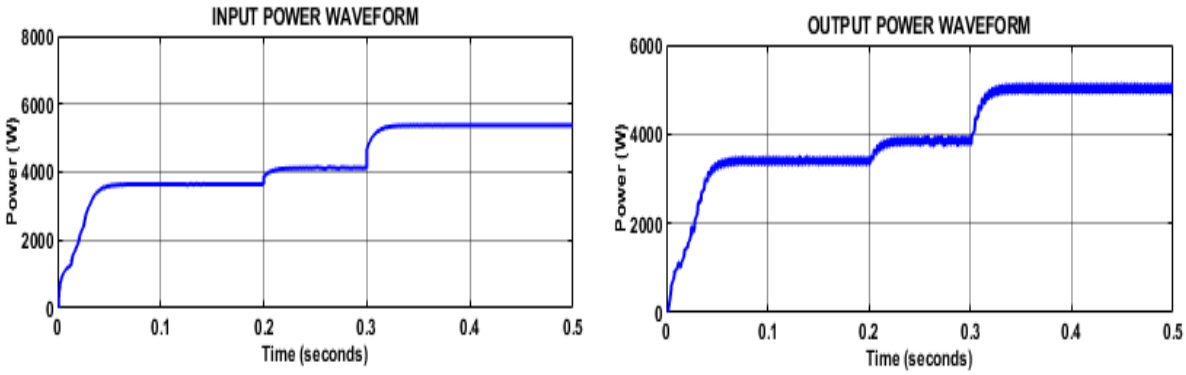

Fig. 11. Power response of PV and Converter

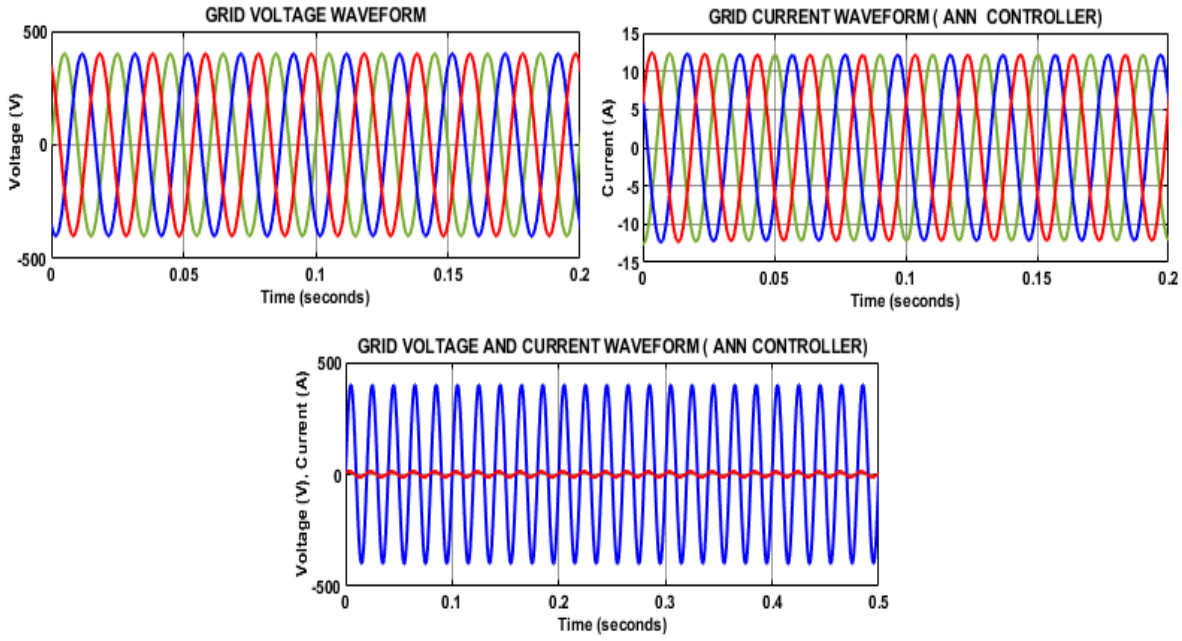

Fig. 12. Grid Waveforms.

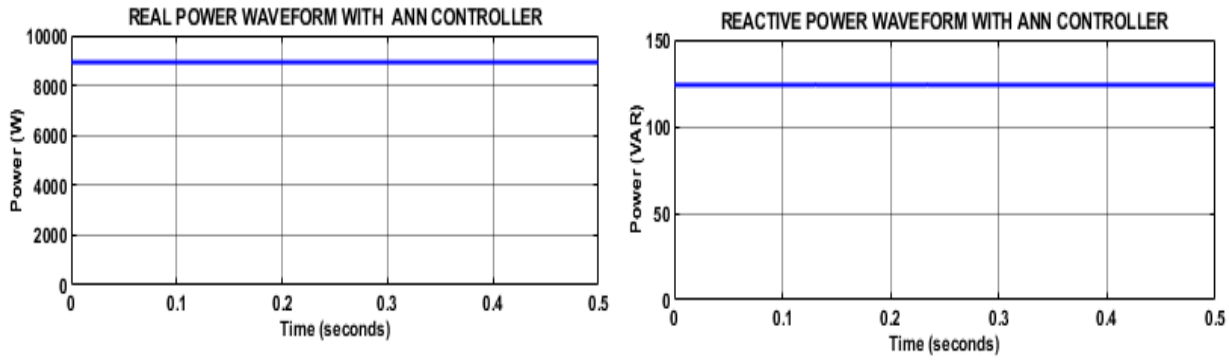

Fig. 13. Real and Reactive Power Waveform with ANN Controller.

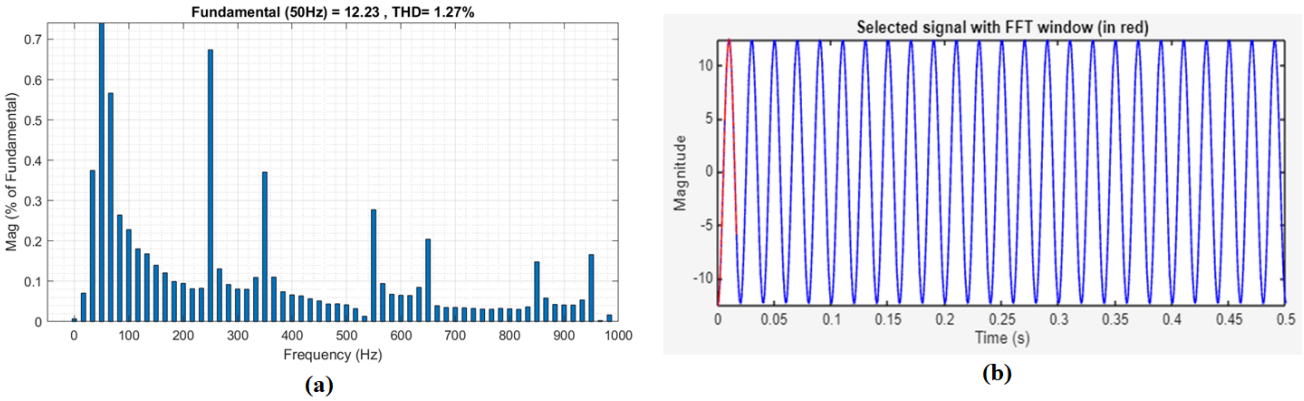

Fig. 14. THD Waveform and FFT plot of Grid Current.

In assistance with ANN-based DQ theory, the proposed system maintains a stable real power output, with minimal fluctuations, demonstrating efficient system regulation. Whereas the reactive power remains low, revealing a near unity power factor with minimized losses in energy, shown in Figure 13.

Figure 14(a) contains the grid current waveform and the actual measured THD. The dq-ANN controller has maintained a current sinusoidal and well synchronized with the grid voltage, exhibiting limited distortion. The THD value is maintained to be 1.27%, exceeding the IEEE 519 limit of 5%, confirming reliable grid integration with excellent power quality. Low distortion also shows superior suppression of higher-order harmonics, which means stable operations with disturbances. Figure 14 (b) indicates the segment of the grid current signal that is selected by the authors for FFT analysis. The sinusoidal shape represents the steady-state grid current, and the area highlighted in red depicts the sampling window for the computation of the Fast Fourier Transform. This ensures that the harmonic spectrum is assessed while operating under steady conditions and therefore provides an accurate reading of the distortion level on current.

5- Comparative Analysis

The comparison efficiency for different converter topologies is represented in Figure 15. The proposed ZSBC accomplishes the highest efficiency of 96.42%, outperforming the high step-up switched Z-source [20] with 83.1%, quasi Z-source converter [21] with 94%, and switched Z-source [22] with 94.2%, making it superior for renewable energy applications.

The comparative analysis of various MPPT techniques utilized for tracking of PV power is demonstrated in Figure 16. Hill climbing [23] has the lowest tracking efficiency of 86.40%, variable step incremental conductance [24] achieves 96%, and variable step P&O [25] accomplishes 90.50%. The proposed Cascaded ANFIS MPPT demonstrates the highest efficiency of 98.54%, outperforming existing techniques owing to its adaptive intelligence, enabling accurate and faster tracking of MPP.

The convergence speed of the comparison of ANFIS and Cascaded ANFIS MPPT is represented in Figure 17. The cascaded ANFIS MPPT outperforms the traditional ANFIS MPPT owing to its multi-stage structure, with fine adjustment allowing for faster tracking of MPP. Moreover, it

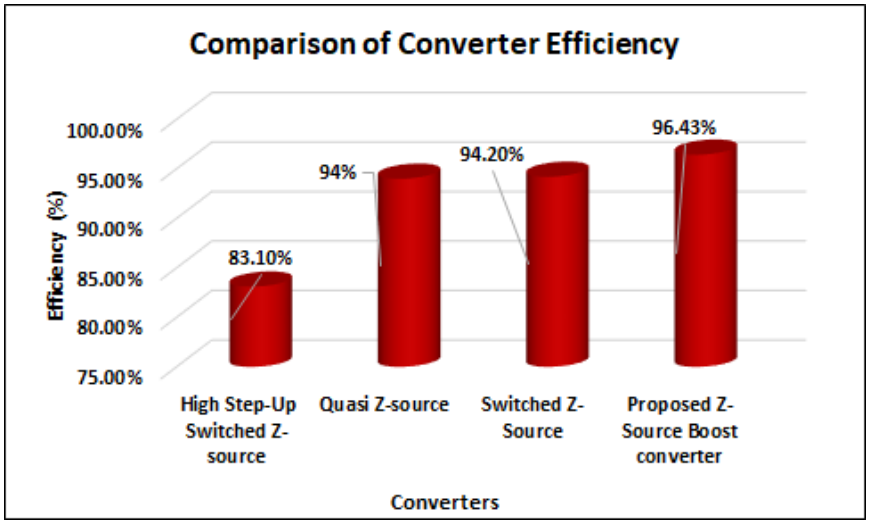

Fig. 15. Comparative Analysis of Converter Efficiency.

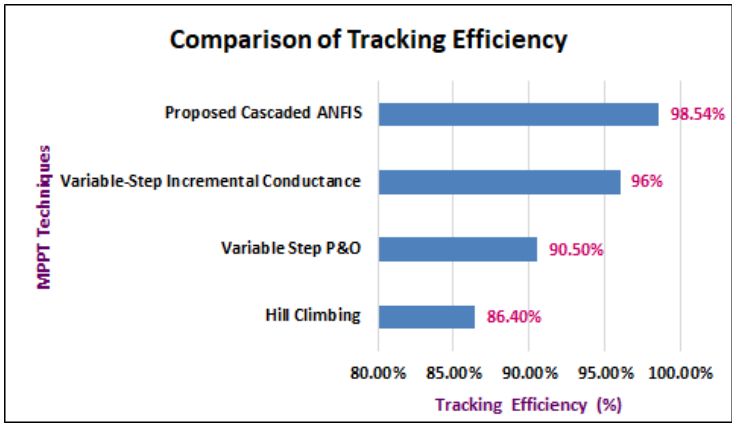

Fig. 16. Comparison of MPPT Tracking Efficiency.

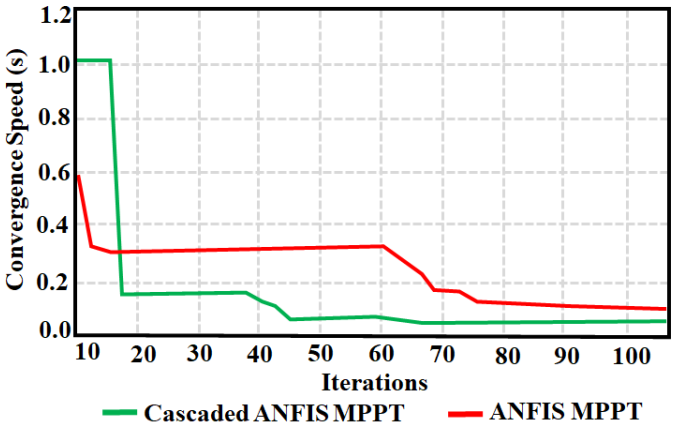

Fig. 17. Comparison of MPPT Tracking Efficiency.

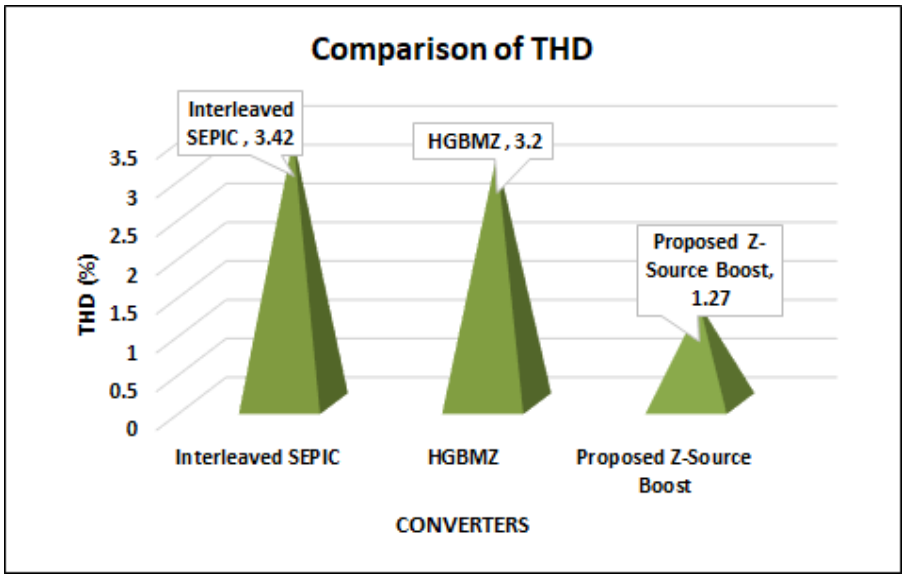

Fig. 18. THD Assessment.

Table 3. Comparison of Converter's Components Count.

CONVERTERS	High step-up [28]	Interleaved quadratic Boost [29]	Interleaved high gain boost [30]	Proposed
SWITCH	1	2	2	1
CAPACITOR	4	3	5	4
INDUCTOR	2	3	2	2
DIODE	4	4	5	2
TOTAL COMPONENTS	11	12	14	9
EFFICIENCY (%)	95.2%	96%	96%	96.42%

reduces the iterations and avoids local optima, allowing for faster stabilization.

The evaluation of THD for various converters is illustrated in Figure 18, the graph displays that the Z-source Boost converter reaches the lowest THD of 1.27%, together with the assistance of an ANN controller based dq theory, overtaking other converters like Interleaved SEPIC [26] with 3.42% and High Gain Bidirectional Modified Zeta (HGBMZ) [27] with 3.2%, respectively.

Table 3 presents a review of proposed converters with other state-of-the-art high-gain converter topologies based on components used and the efficiencies achieved. The results show that the proposed converter used fewer components (only 9) than the alternatives while also providing the greatest efficiency of 96.42%. Fewer components achieved the benefits of lower conduction losses, lower cost, and more reliability. As well, the proposed converter utilized one switch with arranged passive components to lessen voltage stress and increase power density.

Figure 19 compares the duty cycle and voltage gain for the proposed ZSBC, and three more recent high-gain designs - High Step-Up [28], Interleaved Quadratic Boost [29], and Interleaved High Gain Boost [30]. The proposed converter comparatively provides more gain at lower duty cycles than conventional topologies, but also allows the application to reduce switching stress and increase efficiency. This property emphasizes the advantages of the proposed topology since PV applications require low input voltage and high boosting capability. While the voltage gain of the proposed ZSBC increases dramatically beyond duty ratios greater than 0.6, the system is intentionally kept within the stable range of 0.35-0.55. Furthermore, the Cascaded ANFIS MPPT enables seamless duty cycle transitions, while the impedance network automatically reduces current spikes, eliminating control instability while retaining dynamic robustness.

Figure 20 shows switch and diode voltage stress for four converter types: High Step-Up [28], Interleaved Quadratic Boost [29], Interleaved High-Gain Boost [30], and the

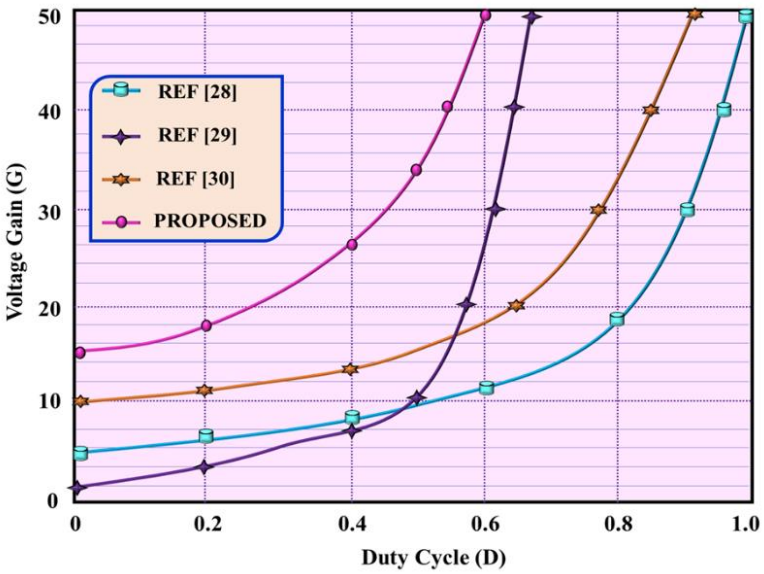

Fig. 19. Comparison of converters' voltage gain.

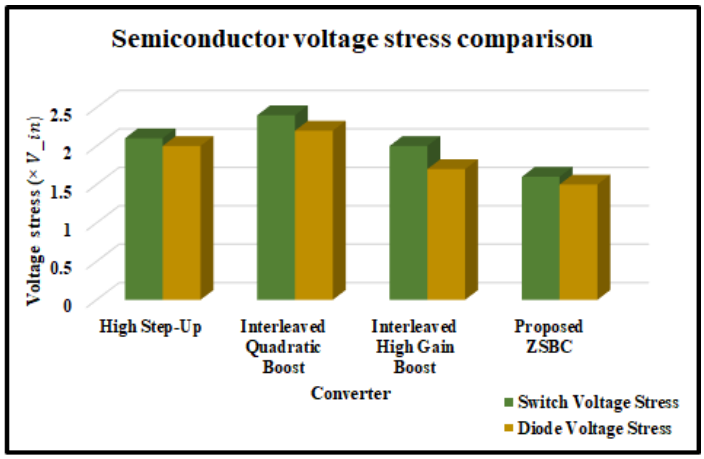

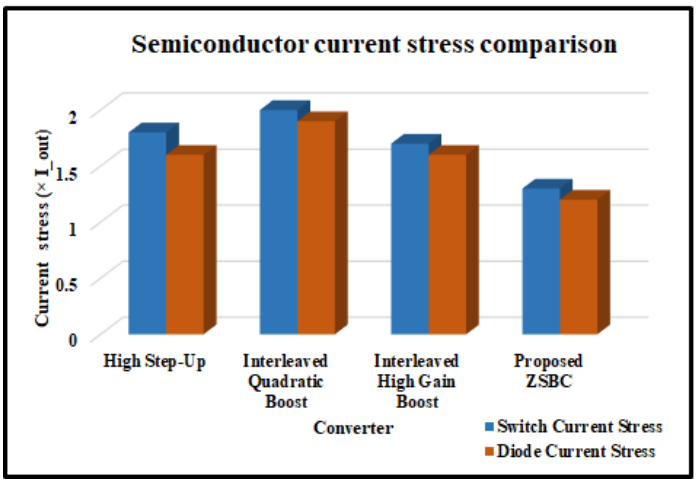

Fig. 20. Comparison of voltage and current stress.

proposed ZSBC. Conventional converters have higher semiconductor voltage and current stress. In comparison, the Proposed ZSBC has the lowest voltage stress for both the switch and the diode, indicating increased device reliability and lower voltage rating requirements. Similarly proposed ZSBC greatly reduces switch and diode current stress. This reduced voltage and current stress helps to reduce conduction losses, improve efficiency, and increase component lifespan.

6- Conclusion

This research proposes a microgrid system, incorporating a Z-Source Boost converter and cascaded ANFIS MPPT and neural network assisted dq theory for the elimination of harmonics. The developed boost converter effectively improves the voltage generated by the PV system, resulting in higher voltage conversion rates, with minimal loss of energy. The Cascaded ANFIS MPPT accurately tracks the MPP, optimizing the extraction of PV energy under varying temperature and irradiance conditions. Simulation results from MATLAB demonstrate that the system achieves a notable converter efficiency of 96.42%, with tracking efficiency of 98.54% by the Cascaded ANFIS MPPT approach. The ANN-based DQ theory further enhances the system's performance by effectively managing the real and reactive power, with THD resulting as low as 1.27%, resulting in high quality of power delivered to the grid. This lower THD, and minimal reactive power output demonstrate that the system operates with minimal harmonics and better power factor, making it suitable for grid integration.

References

[1] A. Kumar, M. Alaraj, M. Rizwan, and U. Nangia, "Novel AI-Based Energy Management System for Smart Grid with RES Integration", In IEEE Access, vol. 9, Nov. 2021, pp. 162530-162542.

[2] J. K. Singh, K. A. Jaafari, R. K. Behera, K. A. Hosani, and U. R. Muduli, "Faster Convergence Controller With Distorted Grid Conditions for Photovoltaic Grid Following Inverter System", In IEEE Access, vol. 10, Mar. 2022, pp. 29834-29845.

[3] A. I. M. Ali, H. H. Mousa, H. R. Mohamed, S. Kamel, A. S. Hassan, Z. M. Alaas, E. E. Mohamed, and A. R. Abdallah, "An Enhanced P&O MPPT Algorithm with Concise Search Area for Grid-Tied PV Systems", IN IEEE Access, vol. 11, Jul. 2023, pp. 79408-79421.

[4] K. S. Kavin, P. Subha Karuvelam, M. Devesh Raj, and M. Sivasubramanian, "A Novel KSK Converter with Machine Learning MPPT for PV Applications", Electric Power Components and Systems, Apr. 2024, pp. 1-19.

[5] M. A. Hassan, C. L. Su, F. Z. Chen, and K. Y. Lo, "Adaptive Passivity-Based Control of a DC–DC Boost Power Converter Supplying Constant Power and Constant Voltage Loads", IEEE Transactions on Industrial Electronics, vol. 69, no. 6, June 2022, pp. 6204-6214.

[6] K. Wang, D. Liu, and L. Wang, "The implementation of synergetic control for a DC-DC buck-boost converter," Procedia Computer Science", vol. 199, Jan. 2022, pp. 900-907.

[7] H. Gholizadeh, S. A. Gorji, E. Afjei, and D. Sera, "Design and implementation of a new cuk-based step-up DC–DC converter", Energies, vol. 14, no. 21, Oct. 2021, pp. 6975.

[8] E. Madrid, D. Murillo-Yarce, C. Restrepo, J. Muñoz, and R. Giral, "Modelling of SEPIC, ćuk and zeta converters in discontinuous conduction mode and performance evaluation", Sensors, vol. 21, no. 22, Nov. 2021, pp. 7434.

[9] N. Subhani, Z. May, M. K. Alam, I. Khan, M. A. Hossain, and S. Mamun, "An Improved Non-Isolated Quadratic DC-DC Boost Converter with Ultra High Gain Ability", IEEE Access, vol. 11, Feb. 2023, pp. 11350-11363.

[10] A. R. Assidiq, A. Dahono, A. Rizqiawan, and Jihad Furqani, "High Ratio DC-DC Converter based on Cascade Modified Cuk Converter Topology", e-Prime-Advances in Electrical Engineering, Electronics and Energy, vol. 9, Jun. 2024, pp. 100654.

[11] M. F. Elmorshedy, I. J. A. Essawy, E. M. Rashad, M. R. Islam, and S. M. Dabour, "A Grid-Connected PV System Based on Quasi-Z-Source Inverter with Maximum Power Extraction", IEEE Transactions on Industry Applications, vol. 59, no. 5, Sep. 2023, pp. 6445-6456.

[12] R. Rahimi, S. Habibi, M. Ferdowsi, and P. Shamsi, "Z-Source-Based High Step-Up DC–DC Converters for Photovoltaic Applications", IEEE Journal of Emerging and Selected Topics in Power Electronics, vol. 10, no. 4, Aug. 2022, pp. 4783-4796.

[13] H. Abouadane, A. Fakkar, D. Sera, A. Lashab, S. Spataru, and T. Kerekes, "Multiple-Power-Sample Based P&O MPPT for Fast-Changing Irradiance Conditions for a Simple Implementation", IEEE Journal of Photovoltaics, vol. 10, no. 5, pp. Sep. 2020, pp. 1481-1488.

[14] A. K. Gupta, R. K. Pachauri, T. Maity, Y. K. Chauhan, O. P. Mahela, B. Khan, P. K. Gupta, "Effect of Various Incremental Conductance MPPT Methods on the Charging of Battery Load Feed by Solar Panel", IEEE. Access, vol. 9, Jun. 2021, pp. 90977-90988.

[15] L. Shang, H. Guo, and W. Zhu, "An improved MPPT control strategy based on incremental conductance algorithm", Protection and Control of Modern Power Systems, vol. 5, no. 2, Jun. 2020, pp. 1-8.

[16] I. Haseeb, A. Armghan, W. Khan, F. Alenezi, N. Alnaim, F. Ali, F. Muhammad, F. R. Albogamy, and Nasim Ullah, "Solar power system assessments using ann and hybrid boost converter based mppt algorithm", Applied Sciences, vol. 11, no. 23, Nov. 2021, pp. 11332.

[17] P. R. Bana, S. D. Arco, and M. Amin, "ANN-Based Robust Current Controller for Single-Stage Grid-Connected PV with Embedded Improved MPPT Scheme", IEEE. Access, vol. 12, Jul. 2024, pp. 100251-100262.

[18] V. Subramanian, V. Indragandhi, R. Kuppusamy, and Y. Teekaraman, "Modeling and analysis of PV system with fuzzy logic MPPT technique for a DC microgrid under variable atmospheric conditions", Electronics, vol. 10, no. 20, Oct. 2021, pp. 2541.

[19] S. A. Ibrahim, A. Nasr, and M. A. Enany, "Maximum Power Point Tracking Using ANFIS for a Reconfigurable PV-Based Battery Charger Under Non-Uniform Operating Conditions", IEEE Access, vol. 9, Aug. 2021, pp. 114457-114467.

[20] R. Kumar, R. Kannan, N. S. S. Singh, G. E. M. Abro, N. Mathur, and M. Baba, "An efficient design of high step-up switched Z-Source (HS-SZSC) DC-DC converter for grid-connected inverters", Electronics, vol. 11, no. 15, Aug. 2022, pp. 2440.

[21] S. Honarmand, A. Rajaei, M. Shahparasti, A. Luna, and E. Pouresmaeil. "A modified partial power structure for quasi Z-source converter to improve voltage gain and power rating", Energies, vol. 12, no. 11, Jun. 2019, pp. 2139.

[22] A. Ahmad, R. K. Singh, and A. R. Beig, "Switched-Capacitor Based Modified Extended High Gain Switched Boost Z-Source Inverters", IEEE Access, vol. 7, Dec. 2019, pp. 179918-179928.

[23] X. Liu, and E. Sánchez-Sinencio, "An 86% Efficiency 12 μW Self-Sustaining PV Energy Harvesting System with Hysteresis Regulation and Time-Domain MPPT for IOT Smart Nodes", IEEE Journal of Solid-State Circuits, vol. 50, no. 6, June 2015, pp. 1424-1437.

[24] H. Ramadan, A. R. Youssef, H. H. H. Mousa, and E. E. Mohamed, "An efficient variable-step P&O maximum power point tracking technique for grid-connected wind energy conversion system", SN Applied Sciences, vol.1, Dec. 2019, pp. 1-15.

[25] N. E. Zakzouk, M. A. Elsaharty, A. K. Abdelsalam, A. A. Helal, and B. W. Williams, "Improved performance low-cost incremental conductance PV MPPT technique", IET Renewable Power Generation, vol. 10, no. 4, Apr. 2016, pp. 561-574.

[26] K. S. Kavin, and P. Subha Karuvelam, "PV-based grid interactive PMBLDC electric vehicle with high gain interleaved DC-DC SEPIC Converter", IETE Journal of Research, vol. 69, no. 7, Sep. 2023, pp. 4791-4805.

[27] Kumar, R. Tharwin, and C. Christober Asir Rajan. "Optimized Hybrid Renewable Energy System for Sustainable Electric Vehicle Charging: Integration of Photovoltaic and Wind Power With Advanced Control Strategies." IEEE Access (2024). Vijaya Chandrakala, K. R. M., Umashankar Subramaniam, and Dhafer Almakhles. "Implementation of high step up converter using RBFN MPPT controller for fuel cell based electric vehicle application." Scientific Reports 14, no. 1 (2024): 1-22.

[28] Ferreira, Daniel, Armando Cordeiro, Paulo Gambôa, Luis Rocha, Filipe Barata, José Fernando Silva, João F. Martins, and Vitor Fernão Pires. "Interleaved Quadratic Boost DC-DC Converter with Extended Voltage Gain and Reduced Switch Voltage Stress for Photovoltaic Applications." Open Research Europe 5 (2025): 55.

[29] Hosseinpour, Majid, Elham Seifi, Ali Seifi, and Shahab Sajedi. "A novel interleaved nonisolated high–gain DC–DC boost converter based on voltage multiplier rectifier." Scientific Reports 15, no. 1 (2025): 26284.

HOW TO CITE THIS ARTICLE

B. K. Santhoshi, D. R. Kishore, Md. Sh. Akhter, A. Iqubal, A. Ali, Design of Three-Phase Grid-Connected PV System with Z-Source Boost Converter and Neural Network-Based Harmonic Elimination, AUT J. Elec. Eng., 58(1) (2026) 189-204.

DOI: 10.22060/eej.2025.24499.5717